Improving methods in X-ray nanotomography of fibre bonds

FYSZ470 Research training, 2017-04-24

Author:

Tuomas Sormunen

Supervisor:

Joni Parkkonen M.Sc.

UNIVERSITY OF JYVÄSKYLÄ
DEPARTMENT OF PHYSICS

Abstract

Tuomas Sormunen
Improving methods in X-ray nanotomography of fibre bonds
FYSZ470 Research training
Department of Physics, University of Jyväskylä, 2017

X-ray nanotomography has proven to be a useful yet challenging method in the study of cellulose fibre bonds. The challenges encountered in previous researches are related to lengthy imaging times and low success rate per sample. To counter these obstacles, fibre staining in order to enhance contrast in radiographic images and an alternative method for marker particle placement were examined in this study. Cesium iodide proved to be a suitable staining material, and the alternative method for particle placement may increase success rate by reducing microfibril structure fracturing during the marker placement process.

Keywords: X-ray, nanotomography, fibre, bond, pulp, cellulose

Contents

1 Introduction

Computed X-ray tomography is a non-invasive imaging method that is used in many different research areas ranging from humans in medical imaging and composite materials in the micro- and nanometer magnitude. The method combines the penetrative ability of high-energy electromagnetic radiation and mathematical algorithms to recreate a 3D reconstruction from individual projection images or radiographs of a sample, acquired from a range of different angles. The inner structure of the sample is represented in the 3D reconstruction slices, from which the areas of interest can be fully analyzed.

1.1 X-radiation

X-radiation is defined as electromagnetic radiation in the wavelength range 0.01 – 10 nanometers [1]. Due to the short wavelength, X-ray energies are relatively high and consequently penetrate many materials well. As such, they can be used to probe the inner structure of many different kinds of samples.

X-rays are generated by the dynamics of charged particles, most notably electrons. In most X-ray sources, electrons are generated in a filament, from which they are accelerated with a potential difference towards a target metal. When the electrons strike the target, they lose energy via interactions with the target atoms. "Bremsstrahlung" (braking radiation) is the phenomenon of accelerated electrons decelarating due to attraction by the positive nucleus of the target atoms. Due to the deceleration, the energies of the electrons change in a wide range, resulting in emission of X-rays with different energies, and a continuous spectrum is produced. The accelerated electron can also deflect a target electron out of its atomic shell. An outer shell electron is promoted to the vacancy of the lower energy shell, releasing energy and producing the so-called characteristic radiation. Characteristic radiation is seen as sharp peaks in the spectrum, with the wavelengths depending on the energy difference between the levels. [1]

Photons penetrating a material obey the Beer–Lambert law which states that the intensity of incoming radiation is attenuated exponentially in a sample. This can be evaluated by the equation

$$I = I_0 \mathrm{e}^{-\mu x}, \tag{1}$$

where I is the intensity of the radiation after the sample, I_0 the incoming radiation, x the thickness of the sample and μ the effective linear absorption coefficient. The absorption coefficient is heavily dependent on the atomic mass of the atoms in the sample material, and also the energy of the photons. Knowing the intensity of the radiation before and

after the sample, it is possible to deduce the attenuation through singular paths of the sample. Strictly, this applies only for monochromatic radiation, but corrective methods can be used so that the polychromaticity is not an obstacle. [2]

1.2 Cellulose fibres

Pulp is the main ingredient in making paper products of various kinds. It is essentially a mix of water and cellulose fibres separated from a variety of wood products. After the pulp undergoes multiple stages of processing, paper is formed from a dense layer of fibre network. The network structure is essentially a product of fibres pressed together to form bonds. The properties of the formed paper product is dependent upon the strength of the inter-fibre bonding, including the total contact area of the fibres. [3]

1.3 Fibre bond imaging

The method of X-ray nanotomography in imaging cellulose fibre bonds has been carried out as a joint project between the VTT Technical Research Centre of Finland and the University of Jyväskylä. The goal of this research was to examine the contact area of two fibres bonded together, and the utilized techniques proved to be advantageous. However, certain challenges were met in conducting the research. [4]

Since cellulose fibres are not very dense and are made of atoms with low atomic masses, high-energy X-rays penetrate the samples with little attenuation. This means the transmission through the sample is very close to the background, producing images with poor contrast since the incoming and outgoing intensities differ only slightly. In order to counter this, the exposure time and image number have to be increased, resulting in a total imaging time of several days.

Since cellulose fibres are very small, rotation of the sample, radiation pressure and thermal interactions due to X-ray absorption may have an effect on the position of the sample during imaging. If the sample does move during imaging, motion artifacts are observed in the 3D reconstruction [5]. Due to these artifacts, the bond area may not be well resolved and as such the contact area cannot be defined precisely.

Considering these facts, generating a large enough data set of successful 3D reconstructions in order to make conclusions about contact areas of bonds of different fibres is tedious. This research training was aimed at developing a method to decrease the total imaging time of the fibre bonds. Different materials to stain the fibres were tested in order to increase the absorption of X-rays in the sample. Additionally, a method to decrease the probability of motion artifacts was developed. Finally, imaging parameter optimization was done to find the ideal exposure time and number of projection images.

2 Equipment

The X-ray nanotomography apparatus used in the study is the Xradia nanoXCT-100. It consists of an X-ray source, focusing optics with a variety of optical components, sample stage and a detector. The configuration produces a parallel beam geometry, i.e. X-rays can be approximated to arrive to the sample from an infinite distance as to generate a plane wave front. The field of view in the large FOV imaging setting is 60 micrometers with 65 nanometer pixel size and 150 nm spatial resolution. As such, it is adequate in the study of samples in the micron-scale.

The X-rays are produced by colliding electrons with a rotating anode with a copper target, with the electron beam having a spot size of approximately 70 micrometres on the anode, producing characteristic radiation at 8 keV. The produced X-rays are optically directed towards the sample in the focus. The detector system behind the sample is essentially made up of a flight tube with magnifying objectives, a scintillator, which converts the incoming X-radiation to visible light via luminescence, tubelens, and a camera. Inside the camera, CCD cells of each pixel records the electric charge due to photoelectric effect induced by the optical photons. The produced radiograph is represented by a digital 2D image with gray values, or counts, being proportional to the intensity of the incoming radiation.

The sample sits on a stage which is rotated between individual radiograph imagings. Since the FOV is small, the rotation process may drive the sample out of the FOV during the steps in the half or full rotation of the sample. As such, the stage is equipped with actuators in all spatial directions in order to correct for these deviations during consecutive rotation steps, keeping the sample in the FOV at all angles. [6]

The chosen imaging parameters, including exposure time, number of radiographs and binning, all have an effect on the resolution of the 3D reconstruction. Using longer exposure times leads to better signal-to-noise ratio since random errors have a lower weight upon a larger mass of data. The number of radiographs, or the number of viewing angles, is correlated with the resolution of details in the sample. Finally binning of camera pixels, i.e. how many camera pixels are grouped together onto a single image pixel, affects the spatial resolution accordingly.

3 Methodology

The method to analyse the contact area of fibre bonds involves 3 main steps. First, fibre bonds have to be made and suitable samples selected to further preparation. After preparation, the sample is imaged. Finally, the acquired radiographs are post-aligned and reconstruction is done, after which image analysis will take place.

3.1 Fibre processing

In order to create fibre bonds, 150 microlitres of diluted HC-LC (high consistency - low consistency) refined pulp fibre suspension was placed between two square-shaped polystyrene plates with side length of 44.3 mm. After this, a pressure of 0.5 bars was applied by placing a 10 kilogram weight on top of the plates for a total of 5 minutes. This was to simulate the paper manufacturing process of wet pressing, upon which the processed pulp is pressurised to produce a thick web. After pressurising, the plates were dried in an 80 °C oven for 1.5 hours so that the excess water evaporates. Suitable fibre bonds, i.e. ones with fibres bonded together as close to 90 degree angle as possible, were selected for preparation. This was to ensure the whole bond area fits into the FOV in the imaging stage.

3.2 Sample preparation

The fibre bond sample is glued to the head of a needle such that the bond area is not obstructed by the tip. This is accomplished with the help of a microscope, micromanipulators and a gripper. Afterwards, fibre branches around the bond area are cut with a UV-laser due to their redundancy. Since objects disappearing and reappearing into the FOV in the imaging is a source of artifacts, cutting the horizontal fibre branches as short as possible is important. Finally, a golden marker particle of size $1.5 - 3.0$ micrometers is placed above the bond using a hair dipped in gold powder.

3.3 Imaging

The sample coordinates are determined with the pre-alignment microscope. The coordinates correspond to those of the sample stage in the imaging apparatus, onto which the sample is placed. The stage is remotely controlled by software, to which the coordinates can be submitted. The attached gold particle can be utilised to calibrate the stage such that upon each rotation angle, a correction value is added to the stage x- and z-coordinates to keep the sample in the FOV. The sample is left on the stage for 4 hours

so that the sample stabilises to the humidity and temperature of the apparatus. During this period, acquisition of reference images takes place. Reference images are used to normalise the gray values of the actual images, since the intensities in the FOV are not identical in every position. 45 reference images are acquired with exposure time half of the actual imaging, and the last 40 images are used to create an average reference image, which is divided pixel-wise from each acquired image. For the first images, the X-ray flux may not have stabilised, so the first five are discarded. After reference imaging and successful calibrations, the imaging parameters are submitted to the software and the sample is imaged from 0 to 180 degrees with binning 1, i.e. each camera cell corresponds to a pixel in the acquired images.

3.4 Post-processing

Since the actuators controlling the stage are not accurate compared to the spatial resolution of the images, and due to wobble of the rotation stage, the sample spatially drifts between rotation step. Thus, the images have to be aligned after imaging to account for these deviations. This is called registering. In short, the coordinates of the centre of the gold particle in each image are used to create an interpolative fit of the rotation. Doing this, a correction can be applied so that the gold particle is in the same coordinate position throughout the images, which makes the reconstruction accurate. If the sample was not exactly on the rotation axis, a centre shift can be applied, i.e. the sample is virtually moved to the correct position. The reconstruction can then take place, if the preview reconstruction slices do not exhibit motion artifacts.

4 Conducted tests and results

Several different factors related to improving the existing methods of fibre bond analysis were studied. These involved staining, marker particle placement and image parameterisation, each of which proved to be important in increasing the success rate of the samples or the resolution of the bond area in the reconstruction.

4.1 Staining

Different staining materials were individually added to the diluted fibre suspension in order to increase the contrast in the X-ray images. The contrast enhancement of the staining is due to the fact that heavier elements are chemically added to the fibres. As mentioned, X-ray absorption is heavily dependent upon density and thus atomic mass, so using stains with relatively heavy elements will increase X-ray absorption and thus contrast in the radiographs.

The main challenge in the staining process proved to be that the stain did not survive the fibre processing stage. Most of the staining materials were totally or partly expelled from the fibre contact area due to the applied pressure (see appendices A and B). The tested staining materials are listed in table 1. Of the tested stains, only cesium iodide (CsI) both survived the processing stage and increased absorption sufficiently.

Table 1: List of tested staining materials and their contrast enhancement properties (see appendix F for exact stain concentrations and staining methods).

Staining material	Contrast enhancement
Acridine orange	None
Phosphotungstic acid (PTA)	Good, but only without pressure
Iron cobalt (FeCo)	Poor
Copper sulphate ($CuSO_4$)	Poor
Copper nitrate ($CuNO_3$)	Poor
Iodine-potassium iodide (I_2KI)	Only without pressure
Ioxaglic acid (Hexabrix)	Poor
Cesium iodide (CsI)	Good

4.1.1 Acridine orange

The previous research used acridine orange as a stain in order to facilitate laser cutting of the fibres, since bare fibres do not absorb UV-radiation well enough. The stain does not increase contrast. The total imaging time of 60 hours in the previous study was deemed too long, so tests were conducted to see if adequate resolution could be accomplished by

changing the binning value from 1 to 2. Since in using binning 2, 4 camera pixels are grouped to 1 pixel in the formed radiograph, the total imaging time could be reduced down to 15 hours by using the same number of images of 1081 but reducing the exposure time from 180 to 50 seconds. The contrast in the images is quite poor, and as such samples stained with acridine orange are only suitable for longer total imaging times (see appendix A).

4.1.2 Phosphotungstic acid

Before discovering CsI, phosphotungstic acid (PTA) yielded good contrast improvement, but as mentioned, does not survive the pressure stage in fibre processing. Due to this, samples stained with PTA were prepared without pressure and oven drying to see if bonds could be manufactured. Drops of PTA-stained fibre suspension were placed on the plates, and only the other plate was used as a weight on top. The fibres were dried with the plate as pressure in a fume hood for 2 days.

The fibres stayed bonded such that imaging could take place. However, it was found that the shapes of the samples were not uniform (see appendix A). Many of the fibres were only partially in contact with each other, some even sharing no contact area, persevering only due to microfibril entanglement. The bond area did not appear flat in many cases, and the lumen, the hollow centre of the fibres, seemed not to have collapsed. Even if image analysis for these samples was possible, it was established that the pressurisation has to take place in order to have intercomparable results.

4.2 Particle placement

The problem of movement of the sample during imaging was hypothesised to be partly due to the sample bending in the process of placing the gold particle. The particle is placed on the sample using a hair dipped in gold powder. In the previous studies, the sample was touched by the hair in the particle placing process, which may bend the sample, breaking some of the microfibril structures in the fibres. Due to this, rotation in the machine and interaction with the X-rays could more easily result in motion artifacts. This was established in a standardised test. First, the gold particle was placed on the sample without bending it with the hair, i.e. the hair was brought close to the sample and only the cluster of gold grazed the sample surface, with the electrostatic attraction between the cluster and the fibre detaching the particle. The sample was then imaged and reconstructed. Afterwards, the previously used method of touching the fibre with the hair was simulated upon the same sample with the help of a needle, and another imaging took place.

From a single slice in the same position of the fibre, it was evident that the first reconstruction has very little to no motion artifacts in the image, whereas the second reconstruction is quite heavily affected by them (see appendix C). Due to this, the second reconstruction is unanalysable. These results seem to support the hypothesis that gold particle placement plays an important role in motion artifact formation, since all the other parameters and variables were kept identical in both imaging procedures.

4.3 Imaging parameters

After establishing that cesium iodide works as a stain and that motion artifacts can be reduced by careful particle placement, imaging parameter optimisation was conducted. A successful sample stained with CsI was imaged with different exposure times and numbers of images such that the total imaging time would remain roughly the same. Total imaging time of 18 hours was chosen as a benchmark which proved to yield analysable results in CsI staining tests. As both the number of images and exposure time are known to affect the spatial resolution of the reconstruction in X-ray tomography [5], an ideal relation between them will improve the accuracy of the image analysis stage. 4 different settings were used: 361 images with 180 second exposure time, 541 images with 120 seconds, 721 images with 90 seconds, and 1081 images with 60 seconds.

From the results, a certain trend is observed: the greater the number of images, the greater the amount of visible artifacts in the background and the lower the resolution in the sample (see appendix D). However, the standard deviation of the background is lowest in the shortest exposure time and highest in the longest. (see appendix E). This suggests that the reason for lower spatial resolution with increasing image number may be the result of the registering process: Since the exposure time is shorter, the noise in an individual image particularly around the gold particle is greater than in images with longer exposure times. Thus, the exact position of the centre of the particle is more difficult to define and register. This may lead to a systematic error in the alignment, resulting in artifacts in the reconstruction.

The aforementioned trends are particularly apparent from slices toward the top of the sample, near the gold particle, but less so toward the middle. The edges of the FOV produce less accurate data due to the X-ray beam intensity having a maximum at the centre and decreasing towards the edges, which possibly causes the blurring of reconstruction images toward each end of the stack, since the signal-to-noise ratio is lower in those areas throughout the imaging process. The data seems to suggest that lower exposure times indirectly exacerbate this attribute, and as such greater exposure times may generate less blurring.

5 Conclusions

The technique of X-ray nanotomography has proven to be an efficient tool in the research of cellulose fibre bonds. However, the challenges in producing large amounts of data points hinder this kind of study. Long scanning times are needed for bare fibres, and the probability of motion artifacts ruining the reconstruction seems quite high for samples in the micrometer magnitudes. An additional source of error is the registering of the images: due to the fact that the sample drifts during each rotation step, the images need to be aligned with the help of a high-absorbing marker particle. Since the registering is done by hand, errors may occur in the tracking of the exact centre of the particle.

The problem of long imaging times can be countered with the use of a staining material capable of surviving the fibre processing stage. As the contrast is enhanced by the staining materials, lower exposure times on each rotational step is required to produce an analysable reconstruction. Careful placement of the marker particle yields a decreased amount of microfibril fractures in the fibres, resulting in lower probability of sample movement during imaging and consequently less motion artifacts in the reconstruction. Finally, the image registering process can be made more accurate via longer exposure times.

Overcoming the challenges encountered in the imaging process, fibre bond research using X-ray nanotomography can be significantly improved. Using the aforementioned methods for staining, marker particle placement and imaging parameterisation, data can be acquired with greater speed and higher success rate. As such, consequent fibre bond research employing these methods could provide more accurate and swift results.

References

[1] D. R. Dance, S. Christofides, A.D.A. Maidment, I. D. McLean & K. H. Ng, *Diagnostic radiology physics: A handbook for teachers and students* (IAEA 2014).

[2] S. R. Stock, *Microcomputed Tomography: Methodology and applications* (Taylor & Francis Group LLC, 2009).

[3] K. Niskanen, *Paper Physics (Papermaking Science and Physics)* (Fapet Oy, 1998).

[4] E. Retulainen, J. Parkkonen, A. Miettinen, "X-ray nanotomography of fibre bonds", *Progress in Paper Physics Seminar 2016 Conference Proceedings* (Darmstadt, 2016).

[5] J. T. Bushberg, J. A. Seibert, E. M. Leidholdt Jr. & J. M. Boone, *The essential physics of medical imaging, 2nd edition* (Lippincott Williams & Wilkins, 2002).

[6] *Xradia nanoXCT Laboratory Tool User Manual, version 1.0* (Xradia Inc, 2009).

Appendices

The following image parameterization terms are shortened in the appendices for brevity: s for seconds, b for binning and im for images.

Appendix A: Reconstruction slices of samples with different stains.

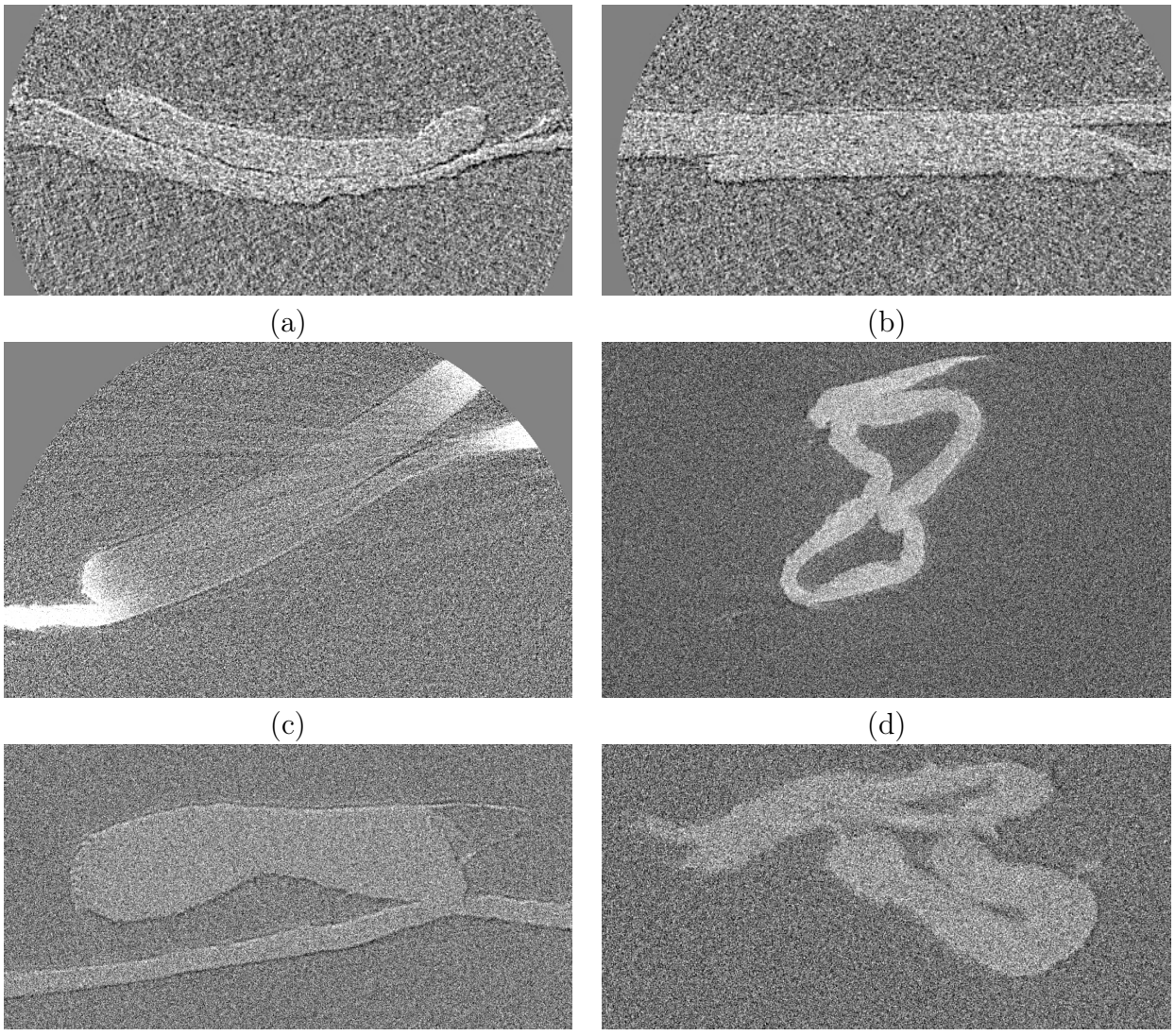

Figure 1: Reconstruction slices of stained samples: acridine orange with parameters (a) 50s, b2, 1081im and (b) 60s, b2, 901im; PTA with parameters 180s, b1, 361im (c) with pressure and (d) – (f) no pressure.

Appendix B: Normalized radiographs of samples with different stains.

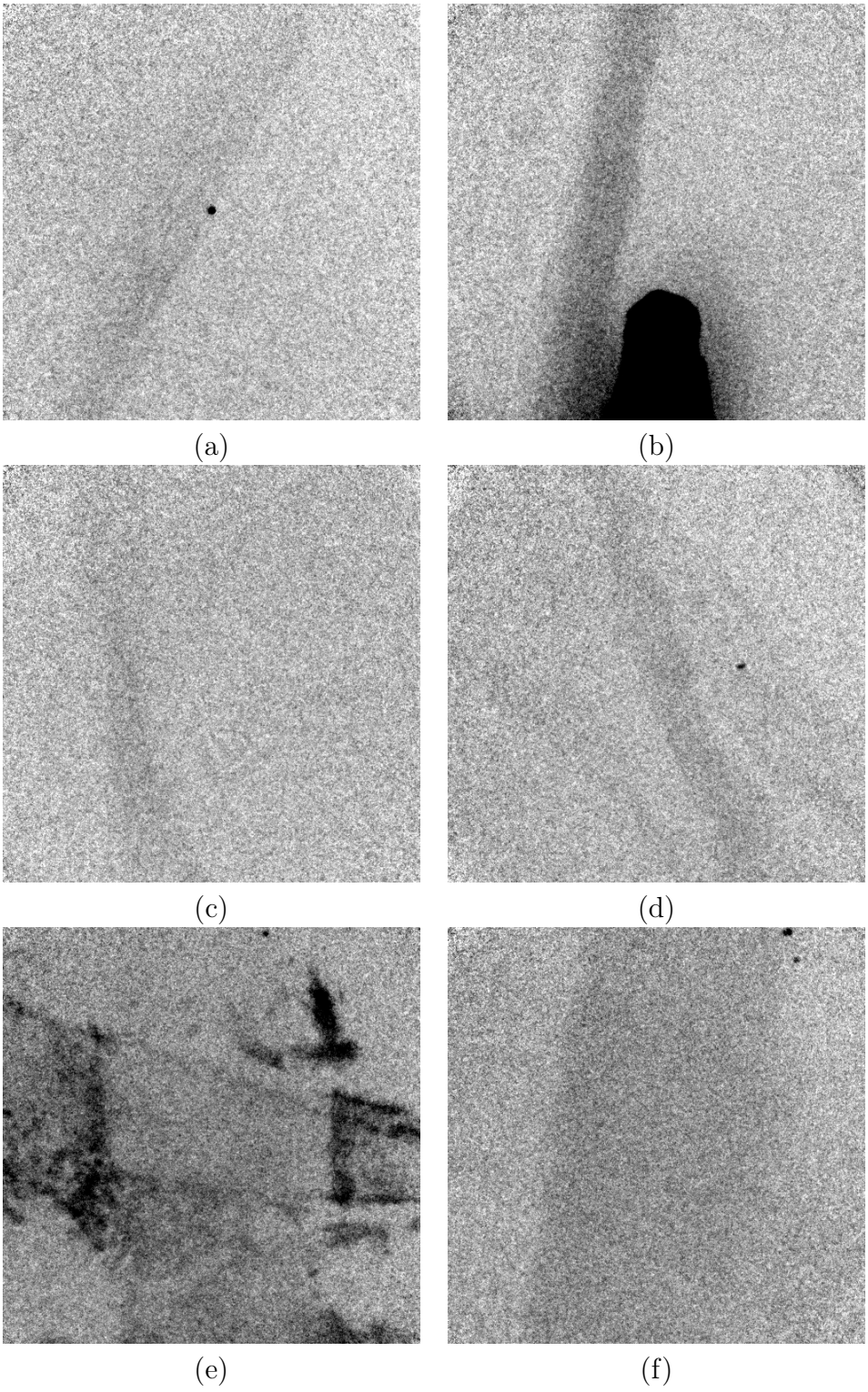

Figure 2: Radiographs of stained and pressurized samples, imaged with parameters 20s, b2: (a) iron cobalt, (b) copper sulphate (with needle visible in black), (c) copper nitrate, (d) iodine-potassium iodide, (e) ioxaglic acid and (f) cesium iodide.

Appendix C: Reconstruction slices of the same acridine orange stained sample.

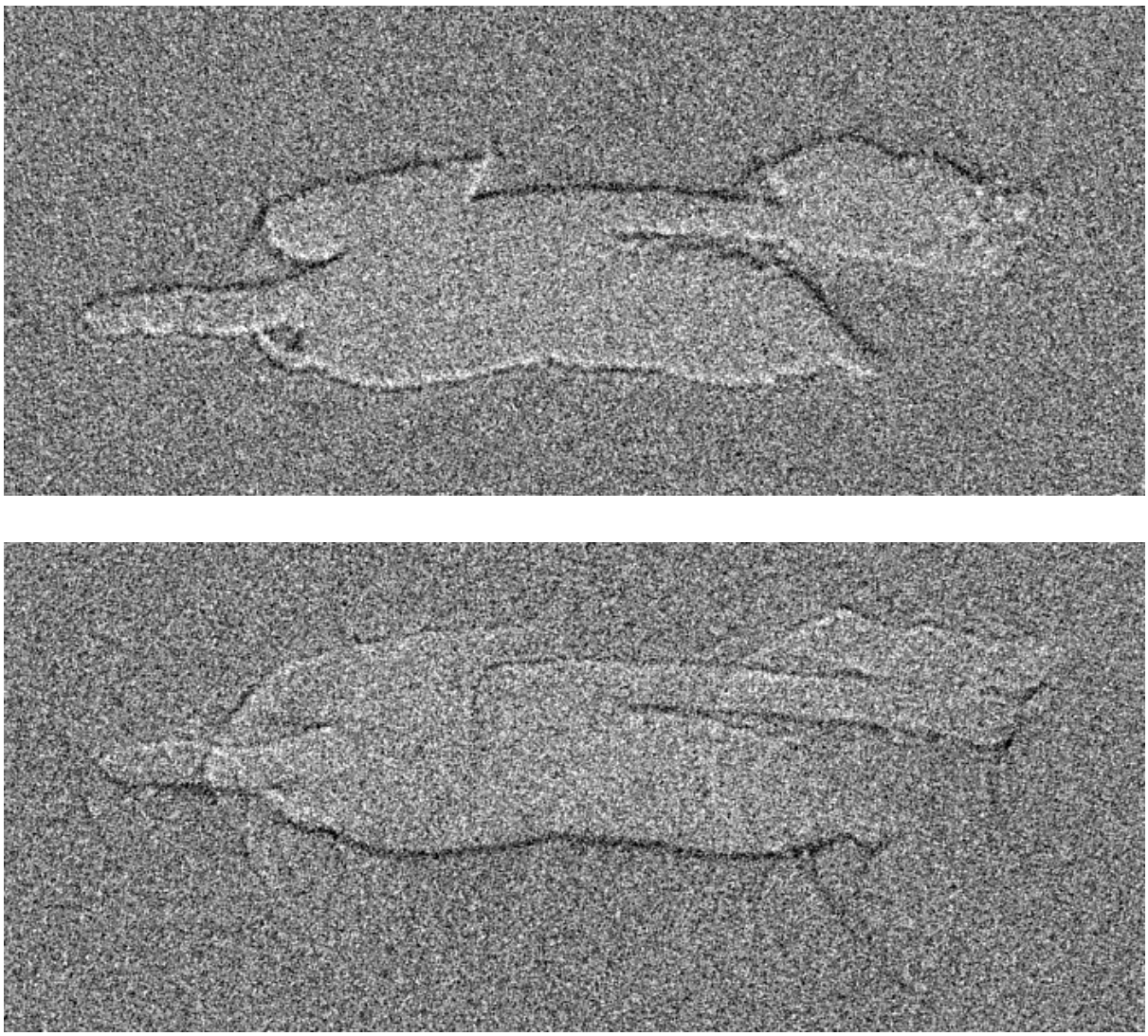

Figure 3: Single reconstruction slices of the same acridine orange stained sample with different gold particle placement methods: slight touch method (top) and the method used in the previous study (bottom).

Appendix D: Reconstruction slices of a single CsI stained sample imaged with different parameters.

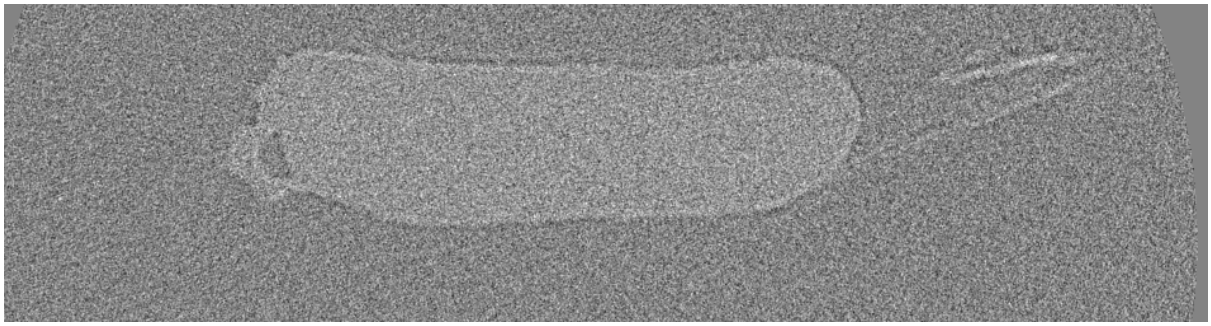

CsI, 180s, b1, 361im.

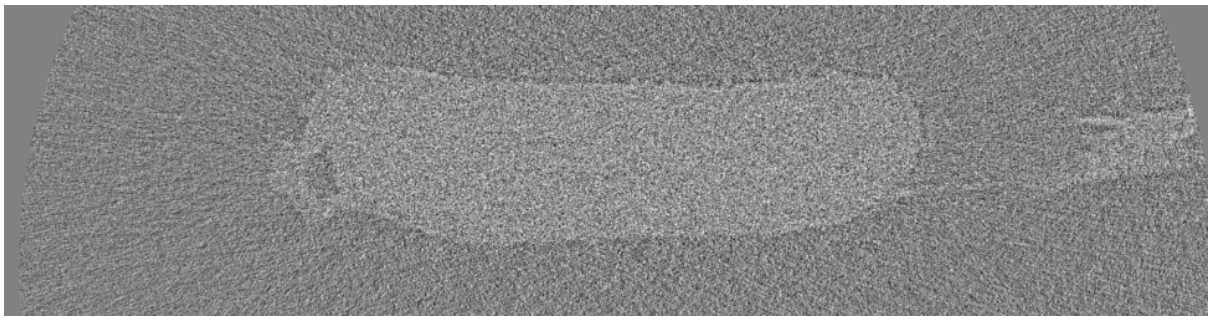

CsI, 120s, b1, 541im.

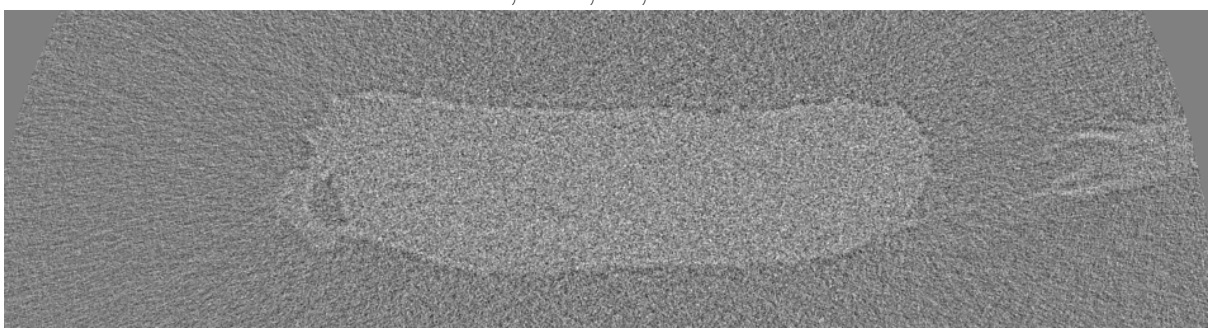

CsI, 90s, b1, 721im.

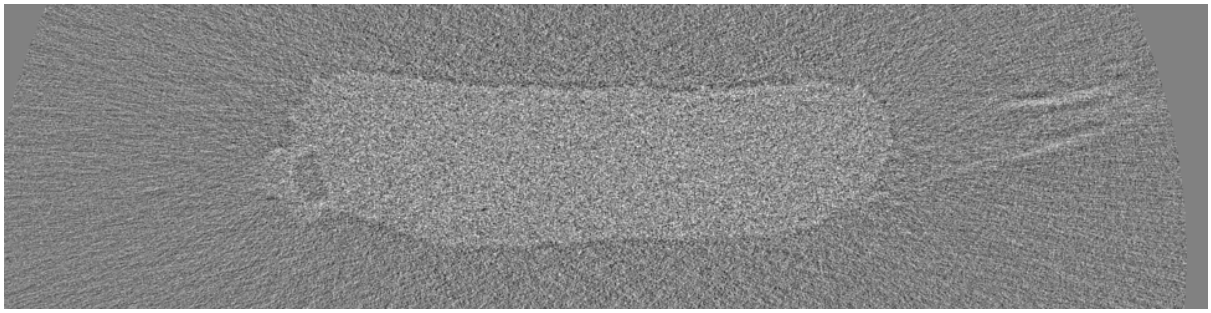

CsI, 60s, b1, 1081im.

Figure 4: Single reconstruction slices of the same CsI-stained sample with different image parameterizations.

Appendix E: Image data of the reconstruction slices of CsI stained samples with different parameterizations.

Table 2: Means and standard deviations of a rectangular 100 by 60 pixel area of the background and the fibre in the single reconstruction slices of figure 4.

	Fibre		Background	
Parameters	Mean	Standard deviation	Mean	Standard deviation
361im, 180s	148.428	23.945	132.523	22.829
541im, 120s	143.749	23.131	128.518	20.549
721im, 90s	145.002	25.219	129.845	20.995
1081im, 60s	144.702	24.891	128.878	20.000

Table 3: Means and standard deviations of a rectangular 200 by 80 pixel area of the background and the fibre in single reconstruction slices, taken from a single image in the middle of each stack.

	Fibre		Background	
Parameters	Mean	Standard deviation	Mean	Standard deviation
361im, 180s	150.470	23.199	132.043	22.800
541im, 120s	147.735	24.299	129.173	22.022
721im, 90s	146.303	23.265	128.189	21.183
1081im, 60s	147.959	24.817	128.787	21.319

Appendix F: The exact methods of fibre staining with each material.

Methods developed by and presented courtesy of Annika Ketola, M.Sc., VTT Technical Research Centre of Finland.

Acridine orange (molar mass = 369.94 g/mol)

Staining solution: 0.00005M acridine orange + 0.01% fibre suspension (1000 ml), 10 min staining time. Afterwards fibres are washed off of excess stain (purified water) and diluted to 0.3% fibre suspension. Bond preparation: 0.3% original solution diluted (1:4) and pipetted.

PTA (molar mass = 2880.2 g/mol), two different preparation methods

3% PTA + 0.3% fibre suspension, (V = 10 ml), staining overnight. Dilution (1:4) for bond preparation (as before).

0.3% fibre suspension + 1% starch Raisamyl 50027 (amount of starch added is 1% of the mass of the fibres) + 3% PTA, (V = 10 ml). Starch is washed off before adding stain. 0.3% fibre suspension diluted (1:4) for bond preparation.

FeCo[1]

0.7% fibre suspension + 0.1M $FeSO_4$ + 0.05M $CoCl_2$ (V = 100 ml). After staining the fibres are washed off of excess stain and diluted to 0.3% suspension. Dilution (1:4) for bond preparation.

$CuSO_4$, two different preparation methods[2]

0.7% fibre suspension + 0.005M $CuSO_4$ (V = 100 ml). 1) The staining solution was warmed for 60 min in 95 °C. 2) Staining at room temperature overnight. After staining the fibres are washed off of excess stain and diluted to 0.3% suspension. Dilution (1:4) for bond preparation.

[1]FeCo staining method adapted from the following Master's thesis:
L. Ruusuvirta, *Microfibrillated cellulose – structure, properties and interactions with metals* (University of Jyväskylä, Department of Chemistry Laboratory of Inorganic and Analytical Chemistry, 2012).

[2]Copper based staining methods adapted from the following articles:
E. Norkus. et al., "Interaction of copper(II) with cellulose pulp" Chemija (Vilnius). 2002. T. 13, Nr.2, and
N. Kotelnikova. et al., "Novel Approaches to Metallization of Cellulose by reduction of cellulose incorporated copper and nickel ions" Macromol. Symp. 2007, 254, 74–79.

$CuNO_3$, two different concentrations[3]

0.7% fibre suspension + 0.002M $CuNO_3$ (V = 100 ml) . After staining the fibres are washed off of excess stain and diluted to 0.3% suspension. Dilution (1:4) for bond preparation.

0.7% fibre suspension + 0.005M $CuNO_3$ (V = 100 ml). After staining the fibres are washed off of excess stain and diluted to 0.3% suspension. Dilution (1:4) for bond preparation.

I_2-KI

0.3% fibre suspension + 1% starch Raisamyl 50027 (amount of starch added is 1% of the mass of the fibres) + 0.1 M KI-I_2 (V = 10 ml). Starch is washed off before adding stain. 0.3% fibre suspension diluted (1:4) for bond preparation.

Ioxaglic acid (molar mass = 1268.88 g/mol)

0.3% fibre suspension + 2% Ioxaglic acid (V = 1 ml), staining overnight. Dilution (1:4) for bond preparation.

CsI

3% CsI + 0.3% fibre suspension, (V = 10 ml), staining overnight. Dilution (1:4) for bond preparation.

[3]See footnote 2.